Tracking down the molecular architecture of

the synaptonemal complex by expansion microscopy

Fabian U. Zwettler[#1], Marie-Christin Spindler[#2], Sebastian Reinhard[1], Teresa Klein[1], Andreas Kurz[1], Markus Sauer*[1], and Ricardo Benavente*[2]

[1]Department of Biotechnology and Biophysics, Biocenter, University of Würzburg, Am Hubland, 97074 Würzburg, Germany

[2]Department of Cell and Developmental Biology, Biocenter, University of Würzburg, Am Hubland, 97074 Würzburg, Germany

[#]These authors contributed equally to this work

Correspondence and requests for materials should be addressed to M.S. and R.B. (m.sauer@uni-wuerzburg.de and benavente@biozentrum.uni-wuerzburg.de)

Abstract

The synaptonemal complex (SC) is a meiosis-specific nuclear multiprotein complex that is essential for proper synapsis, recombination and segregation of homologous chromosomes. We combined structured illumination microscopy (SIM) with different ExM protocols including U-ExM, proExM, and magnified analysis of the proteome (MAP) to investigate the molecular organization of the SC. Comparison with structural data obtained by single-molecule localization microscopy of unexpanded SCs allowed us to investigate ultrastructure preservation of expanded SCs. For image analysis, we developed an automatic image processing software that enabled unbiased expansion factor determination. Here, MAP-SIM provided the best results and enabled reliable three-color super-resolution microscopy of the SCs of a whole set of chromosomes in a spermatocyte with 20-30 nm spatial resolution. Our data demonstrate that post-expansion labeling by MAP-SIM improves immunolabeling efficiency and allowed us thus to unravel previously hidden details of the molecular organization of SCs.

65   Imaging technologies are central platforms that drive fundamental research in virtually all
66   disciplines across the biological and medical sciences. However, the diffraction barrier of
67   classical fluorescence microscopy has hindered obtaining high-resolution information about the
68   molecular architecture of protein assemblies and their interrelations. So far, only electron
69   microscopy (EM) techniques provided a spatial resolution enabling the investigation of the
70   molecular composition and structure of multiprotein complexes[1]. Super-resolution microscopy
71   methods now can provide spatial resolution that is well below the diffraction limit of light
72   microscopy approaching virtually molecular resolution[2,3]. Physical expansion of the cellular
73   structure of interest represents an alternative approach to bypass the diffraction limit and
74   enables super-resolution imaging on standard fluorescence microscopes. For this purpose,
75   expansion microscopy (ExM) has been developed and successfully applied to visualize cellular
76   structures with ~ 70 nm lateral resolution by confocal laser scanning microscopy[4].

77   The original ExM protocol used functionalized antibody-oligonucleotide conjugates that bind to
78   target proteins and cross-link covalently into a swellable hydrogel during polymerization. After
79   degradation of native proteins by enzymatic proteolysis, the sample expands ~4.5-fold in water[4].
80   To circumvent fluorophore loss during polymerization and protease digestion alternative ExM
81   protocols have been introduced enabling imaging of proteins, RNA, and bacteria in cultured
82   cells, neurons, and tissues also in combination with super-resolution microscopy[5-11]. For
83   example, protein-retention ExM (ProExM)[6] and magnified analysis of the proteome (MAP)[7] have
84   been developed that cross-link proteins themselves into the polymer matrix. Replacing protein
85   digestion by heat and chemical induced denaturation allows post-expansion immunolabeling of
86   chemically embedded proteins. To further increase the achievable resolution, the expansion
87   factor has been increased up to 20-fold[12,13]. However, such high expansion factors dramatically
88   reduce the labeling density and consequently also the achievable structural resolution and
89   require ultimately single-molecule sensitive imaging methods to visualize such extremely diluted
90   fluorescence signals. Furthermore, some doubts remained concerning uniform three-
91   dimensional (3D) expansion and preservation of ultrastructural details especially of multiprotein
92   complexes. Very recently, it has been shown that various expansion protocols do not completely
93   preserve the 3D molecular architecture of centrioles. Only by careful optimization of the
94   expansion protocol ultrastructural details of centrioles could be truthfully preserved by U-ExM[14].

95   In the present study, we tested the suitability of different ExM protocols for investigation of the
96   molecular architecture of mammalian synaptonemal complexes (SCs) by structured illumination
97   microscopy (SIM). With EM[15-19] and single-molecule localization microscopy[20] data available

98   about the distribution of SC proteins, it is ideally suited as a benchmark structure to evaluate
99   isotropic expansion and structure preservation of different ExM protocols.

100   ExM-SIM has already been used to investigate the three-dimensional (3D) organization of
101   *Drosophila* SCs with a lateral resolution of ~ 30 nm[21,22]. To locate expanded sample as close as
102   possible above the coverslip, they had to be dehydrated, cryosectioned into 10 μm sections, and
103   then again expanded and mounted on a coverslip. Finally, SIM with an oil-immersion objective
104   and minimal spherical aberration has been performed. Here, we optimized sample handling to
105   avoid dehydration and cryosectioning steps and enable super-resolution imaging of expanded
106   SCs by SIM. Therefore, we used nuclear spreadings of mouse spermatocytes, a widely used
107   technique to study nuclear proteins, specifically in the field of meiosis. The spreading of the SCs
108   directly onto the surface of the coverslip results in the localization of the proteins close to the
109   coverslip post-expansion and allows the use of a water-immersion objective for imaging of
110   hydrogels without spherical aberrations. Further, we adapted the hydrogel composition that
111   enabled us to completely detach and transfer the entire sample from the glass surface to the
112   hydrogel. These optimizations and the use of SC spreadings enabled isotropic expansion of the
113   sample and multicolor post-expansion epitope labeling with no need for dehydration and
114   cryosectioning, thus providing a quicker, less error prone approach to study the 3D organization
115   of nuclear proteins.

116   Very recently, ExM has been combined with single-molecule localization microscopy by STORM
117   to elucidate the molecular organization of the murine chromosome axis of SCs on nuclear
118   spreadings[23]. Using ExSTORM on 2.7x expanded samples, the authors achieved a lateral
119   resolution of 20-30 nm, similar to the spatial resolution demonstrated previously by *d*STORM
120   imaging of unexpanded SCs[20]. With a ~3-4x expansion factor in combination with a 2-fold
121   increase in spatial resolution provided by SIM, currently Ex-SIM represents the method of choice
122   for 3D multicolor super-resolution imaging of multiprotein complexes such as SCs. Therefore, we
123   developed a robust workflow for Ex-SIM on nuclear spreadings together with an automated
124   image processing software ('Line Profiler') to simplify the implementation of multicolor Ex-SIM
125   and refined data analysis. The developed method allowed us to unravel new details of the
126   molecular organization of SCs.

127

128

129

130

Results and Discussion

Analyzing SIM images of expanded SCs

Synaptonemal complexes (SCs) are meiosis-specific multiprotein complexes that are essential for synapsis, recombination and segregation of homologous chromosomes, resulting in the generation of genetically diverse haploid gametes, the prerequisite for sexual reproduction[24,25]. The SC exhibits an evolutionarily conserved ladder-like organization composed of two lateral elements (to which the chromatin of homologous chromosomes is associated) and a central region. The central region is formed by a central element running between the lateral elements, and numerous transverse filaments connecting the lateral elements and the central element (**Fig. 1**). Early EM 3D reconstructions show the ribbon-like lateral elements (LEs) of the SC spanning across the nucleus while turning around the own axis[18]. In mammals, eight SC protein components have been identified so far: the proteins SYCP2 and SYCP3 of the lateral elements, SYCP1 of transverse filaments and the proteins SYCE1, SYCE2, SYCE3, TEX12 and SIX6OS1 of the central element[24,25]. The assembly of the SC proteins into an elaborate molecular architecture is hereby tightly coordinated with essential meiotic processes and therefore conserved across species[20-25]. Consequently, localization maps of SC proteins are required to unravel the function of the molecular architecture of the SC in synapsis and recombination and thereby the overall success of meiosis.

In order to elucidate the precise molecular architecture of the SC, nanoscale resolution provided by either EM or super-resolution microscopy is required. Using immunolabeling and super-resolution microscopy by *d*STORM the position of different proteins of the SC on nuclear spreadings have been visualized with approximately 20-30 nm lateral resolution. The images revealed that the lateral element protein SYCP3 shows a bimodal distribution separated by 221.6 ± 6.1 nm (SD) (**Fig. 2**)[20]. This value is in accordance with distances measured between the centers of the two ribbons of parallel oriented lateral elements by EM[15-18]. With SC protein distribution data available, structure preservation and uniform expansion of different ExM protocols can now be efficiently evaluated.

We started with immunolabeling of SYCP3, the N-termini of SYCP1 (SYCP1N), and SYCE3 as proteins of the lateral element, the transverse filaments, and the central element of the SC, respectively on nuclear spreadings using three different ExM protocols. To automatically and objectively analyze the average position of fluorescently labeled SC proteins and determine distances between bimodal distributed proteins from cross-sectional profiles, we developed 'Line Profiler', an automated image processing software (https://line-

164 profiler.readthedocs.io/en/latest/)[26]. Line Profiler uses several image-processing algorithms to
165 evaluate potential regions of interest. In a first step all structures in the SYCE3 channel are
166 reduced to lines with one pixel width by using a threshold and a skeletonize algorithm. The
167 resulting pixel-coordinates are sorted and fitted with a c-spline. This gives an analytical
168 description of the orientation of SYCE3 and therefore a good approximation for the center (line
169 coordinates) and overall orientation of the helically arranged SYCP3 protein (2-channel mode)
170 (**Supplementary Fig. 1**). Note that it is also possible to determine the orientation with a gradient
171 image of the SYCP3 channel, if the SYCE3 channel cannot be evaluated (1-channel mode)
172 (**Supplementary Fig. 2**).

173 To compute the distance between the SC strands, we applied a floodfill algorithm to the SYCP3
174 channel, leaving only areas embedded in closed shapes unequal to zero. In combination with a
175 distance transform, i.e. a computation of the distance of each point within the area to the nearest
176 point outside, the regions, where the helical structure of the SC is in plane (regions of maximal
177 distance between the strands) are revealed. All line coordinates outside of these areas were
178 discarded. A line profile is subsequently constructed for each remaining line coordinate
179 perpendicular to the derivative of the c-spline. For averaging, the line profiles are post aligned to
180 the center between their peaks. We determined the expansion factors of the different protocols
181 by comparing the distances between the maximum intensities of the two SYCP3 strands of
182 unexpanded and expanded SCs imaged by dSTORM and SIM, respectively (**Fig. 2**). SYCP3
183 bimodal protein distributions of unexpanded SCs imaged with dSTORM resulted in an average
184 strand distance of 222 nm ± 33 nm (SD) consistent with our previous dSTORM data[20]
185 (**Supplementary Fig. 3**).

186

Optimization of SC expansion

188 We tested the pre-expansion labeling protocol proExM[6], and the two post-expansion labeling
189 protocols MAP[7] and U-ExM[14]. Among the three ExM protocols tested MAP outperformed the
190 other protocols resulting in an average peak-to-peak distance of cross-sectional profiles of the
191 SYCP3 signals of 632 ± 73 nm (SD) determined using the 1-channel mode to analyze the cross-
192 sectional profiles (**Methods** and **Supplementary Fig. 2**). With a bimodal distribution separated
193 by 222 nm ± 33 nm (SD) as measured by dSTORM from unexpanded SCs (**Supplementary**
194 **Fig. 3**) the MAP protocol enabled three-color SIM imaging and provided an expansion factor of ~
195 2.9x. U-ExM enabled post-expansion labeling with various fluorophores and three-color SIM but
196 expanded SCs showed structural breaks indicating insufficient incorporation of proteins into the
197 gel matrix (**Supplementary Fig. 4**). U-ExM provided an expansion factor of ~ 2.4x using the 1-

198 channel mode method to analyze the cross-sectional profiles (**Supplementary Fig. 5**). On the

199 other hand, proExM provided the largest expansion factor of ~ 4.0x using the 1-channel mode

200 but pre-expansion labeling resulted in a lower labeling density due to irreversible fluorophore

201 destruction during free-radical polymerization (**Supplementary Figs**. **4** and **5**)[4,6]. Although the

202 extent of irreversible fluorophore destruction during gelation varies across fluorophores

203 multicolor imaging with pre-expansion labeling protocols remains challenging.

204 Furthermore, our MAP-SIM data (**Fig. 3**) show that the molecular architecture of the SCs is fully

205 preserved demonstrating isotropic expansion. At first glance, this result appears surprising in

206 light of our recent study evaluating the structure preservation of centrioles using different

207 expansion protocols[14]. For centrioles, the MAP protocol was unsuited, as MAP-treated centrioles

208 appeared even smaller when compared to unexpanded samples. Therefore, U-ExM has been

209 introduced as a variation of the MAP protocol using weaker fixation that enabled excellent

210 isotropic expansion and preservation of the centriole ultrastructure[14]. The main difference

211 between centrioles and SCs is their biomolecular composition. While centrioles are solely

212 composed of proteins, the SC consists of a tight association between DNA and proteins, which

213 may affect expansion efficiency and isotropy. During fixation both proteins amongst each other

214 as well as proteins and DNA are crosslinked. Possibly expansion of SCs requires stronger

215 fixation conditions than used in the U-ExM protocol and at the same time an increased

216 acrylamide concentration to preserve molecular identity and to enable detachment and full

217 transfer of proteins into the gel. After gelation, the proteins are denatured at high temperatures

218 using sodium dodecyl sulfate (SDS). Apart from denaturation, SDS also confers its negative

219 charge to the proteins[27,28]. As the DNA is negatively charged as well, crosslinked DNA and

220 proteins repel each other. We hypothesize that the repulsion between DNA and proteins

221 facilitates isotropic expansion of SCs when using the MAP protocol with stronger fixation

222 conditions.

223 Overall, MAP-SIM with an optimized gel composition enables isotropic ~ 2.9x expansion,

224 efficient transfer of proteins into the hydrogel and molecular structure preservation of SCs. In

225 combination with a two-fold resolution enhancement of SIM, MAP-SIM provides a similar spatial

226 resolution as *d*STORM[20] but in addition a higher immunolabeling efficiency because of the

227 improved epitope accessibility of post-expansion protocols[14]. Therefore, we used our optimized

228 MAP-SIM approach (**Supplementary Fig. 6**) in all following experiments to investigate details of

229 the molecular architecture of SCs.

230 Previous *d*STORM experiments have shown that the C-terminus of SYCP1 localizes to the inner

231 edge of the lateral element and the N-termini of SYCP1 interact in the central element[20]. These

232   findings are in accordance with recent STORM experiments performed on 2.7x expanded

233   nuclear spreadings[23]. Here, the SYCP1 N-terminus was located in the central element roughly

234   110 nm away from the SYCP3 labeled lateral element (LE) while the SYCP1 C-terminus

235   localized 25 nm more inward to SYCP3, which corresponds to the inner edge of the lateral

236   element[23]. Further, in dSTORM experiments the width of the monomodal localization

237   distributions of the N-terminus of transverse filament protein SYCP1 and the central element

238   protein SYCE3 were determined to 39.8 ± 1.1 nm (SD) and 67.8 ± 2.1 nm (SD), respectively, in

239   frontal views of the SC[20]. The broader signal distribution of SYCE3 localizations indicates that

240   the interaction of SYCP1 and SYCE3 might not be limited to the N-terminus of SYCP1. This is

241   consistent with expanded MAP-SIM protein distributions of 229.3 ± 1.2 nm (SD) (FWHM) for

242   SYCE3 and 161.5 ± 1.3 nm (SD) (FWHM) for SYCP1N analyzed from frontal and lateral views of

243   the SC (**Supplementary Fig. 1**).

244   Since dSTORM requires efficient photoswitching of organic dyes in oxygen depleted thiol-buffer,

245   it is currently limited to two-color experiments, whereby carbocyanine dyes such as Cy5 and

246   Alexa Fluor 647 are the best suited fluorophores[29,30]. In contrast, MAP-SIM provides similar

247   resolution but enables imaging with up to three colors simultaneously without optimization of the

248   photoswitching buffer conditions. The number of available laser lines thus only limits multicolor

249   super-resolution microscopy experiments. Therefore, we immunolabeled the N-terminus of

250   SYCP1, SYCE3, and SYCP3 with the same antibodies as used in the dSTORM experiments in

251   triple-localization MAP-SIM experiment (**Fig. 3**). The MAP-SIM images clearly exhibited similar

252   details of the molecular architecture of SCs as single-molecule localization microscopy of

253   unexpanded samples. In addition, the images confirmed isotropic expansion and preservation of

254   the molecular structure of the SC. Intriguingly, spreading of SCs in combination with MAP

255   allowed us to acquire 3D super-resolution images of large expanded samples, e.g. 100 x 100 x

256   30 μm^3 (200 nm z-steps) by re-scan confocal microscopy (RCM)[31] and 80 x 80 x 15 μm^3 (110

257   nm z-steps) and larger by SIM, i.e. imaging of the SCs of a whole set of chromosomes in a

258   spermatocyte with detailed structural information of single chromosomes (**Fig. 3**).

259

260   **MAP-SIM reveals a complex network organization of the SC central region**

261   MAP-SIM images of lateral views of the SC reveal the topology of the transverse filament protein

262   SYCP1 that is oriented perpendicularly to the lateral element protein SYCP3 and the central

263   element protein SYCE3. dSTORM and immunogold EM images showed a bimodal distribution of

264   the N-terminus of SYCP1 and SYCE3 in twisted areas of the SC[19,20]. EM tomography uncovered

265   a multilayered organization of the central element in insects[32,33]. On the other hand, EM

266   tomography based 3D models of the murine SC recently revealed the absence of a layered

267   organization of the SC central region[34].

268   Therefore, we next analyzed the signal distribution of the N-terminus of the transverse filament

269   protein SYCP1 by MAP-SIM of nuclear spreadings in more detail. In addition to analyzing the

270   distribution of proteins in frontal views, we also generated line profiles of SC proteins from lateral

271   views, i.e. twisted areas of the SYCP3 signal (**Fig. 4** and **Supplementary Video 1**). In

272   agreement with EM tomographic data[34], the signal distributions of the MAP-SIM imaged SYCP1

273   N-terminus and SYCE3 indicated a far more complex distribution of the central region proteins

274   than the bimodal distribution previously described by *d*STORM and immunogold EM[19,20].

275   In traditional immunofluorescence and immuno-EM preparations, antibodies have to compete for

276   epitope accessibility of the densely packed central element. Free epitopes at the core of the

277   central elements are difficult to access for IgG antibodies with a size of 10-15 nm taken that

278   primary antibodies bound to the outer epitopes will shield more central epitopes. Using MAP-SIM

279   epitope accessibility is improved due to the initial physical enlargement of the multiprotein

280   complex before post-expansion labeling. The resulting higher labeling density, specifically at the

281   core of the central element, provides a more fine-grained resolution of the molecular

282   organization of the central element. Hence, MAP-SIM discloses new information about the

283   molecular organization of the SC, particularly that the central element proteins are not organized

284   unambiguously as distinct layers but they form a complex network composed of the transverse

285   filament protein SYCP1 and the central element protein SYCE3 as well as other central element

286   proteins in agreement with recent electron tomographic findings[34].

287

288   **Molecular details of SC axes uncovered by MAP-SIM**

289   One striking morphological feature of the lateral elements, which could not be visualized before

290   by light microscopy, is their occasional splitting into two or more sub lateral elements (subLEs).

291   Variations of subLEs have been observed across species from animals to plants to yeast in

292   various EM preparations (histological sections, whole-mount preparations, spreadings)[15,35-41].

293   Again, the continuous signal distribution of MAP-SIM allowed us to close the existing gap

294   between light microscopy and EM and resolve the splitting of the two SYCP3 strands in murine

295   pachytene spermatocytes (**Fig. 5** and **Supplementary Video 2**). Spermatocytes contain 40

296   chromosomes that synapse as bivalents of homologous chromosomes along the synaptonemal

297   complex in order to recombine. The fully synapsed bivalents hereby span the nuclear space with

298   the two pairs of telomeres residing at distant sides of the nuclear envelope. In the XY pair,

299 synapsis is confined to the pseudo-autosomal region and is therefore incomplete. In autosomes,
300 MAP-SIM resolved a doubling of each of the SYCP3 strands (i.e. LEs) specifically, but not
301 exclusively, at the sites where the helical synaptonemal complex twists (lateral view of the SC)
302 and at the ends of the SYCP3 strands (**Fig. 5** and **Supplementary Video 2**).

303 With progression of prophase I, the degree of fraying at the end of the SYCP3 strands
304 increases. In our experiments, we observed a bifurcation of the SYCP3 ends in mid-pachynema
305 and a fraying of the ends into multiple strands in late pachynema/early diplonema (**Fig. 5** and
306 **Supplementary Video 2**). These observations are in agreement with EM findings of subLEs in
307 murine spreadings[38]. Here, a multistranded organization of the lateral elements that arrange into
308 two compact subLEs through interaction with the two sister chromatids has been proposed[37]. In
309 EM images of silver-stained spreadings of mouse SCs, both axes appeared double or
310 multistranded with a higher frequency of subLEs at unpaired regions[41]. Using MAP-SIM, we
311 resolved for the first time the reported fraying of the axes into SYCP3 positive fibrils by light
312 microscopy. In accordance with the conservation of the subLEs of the autosomes, also the
313 fraying of the XY axes is common in mammals[42,43].

314 In mid-pachynema, the homologs are fully synapsed along the SC. Here, doubling of lateral
315 elements is frequently observed and potentially related to the association with the two sister
316 chromatids of the homologs. In diplonema, desynapsis starts and SCs gradually disassemble. At
317 this stage, the lateral elements appear to disperse into individual SYCP3 fibrils. A strong degree
318 of fraying has also been observed in unpaired regions of the XY pair. In 2014, Syrjänen *et al.*
319 resolved the crystal structure of human SYCP3[44]. They showed that the tetrameric protein is
320 approximately 20 nm long and is organized in an antiparallel arrangement that exposes its N-
321 terminal DNA binding sites at either end. Binding to stretches of DNA, SYCP3 self-assembles
322 into higher-order fibers that resemble the lateral elements in vitro. Based on doubling of the
323 lateral elements observed in EM, it has been speculated that SYCP3 might assemble into one
324 subLE per sister chromatid to prevent recombination between sister chromatids while
325 maintaining chromatin cohesion[45].

326

327

328

329

330

331

Conclusion

332

333 To close the discussion about the preservation of molecular structures and uniformity of

334 expansion, we performed a comparison of the 3D molecular architecture of mammalian SCs as

335 visualized by unexpanded *d*STORM[20] and expanded MAP-SIM. Taking advantage of the similar

336 spatial resolution provided by the two methods, even smallest structural deviations are

337 immediately apparent. We have shown that through isotropic structure preserving expansion

338 combined with SIM, ultrastructural details of SCs can be revealed with standard

339 immunofluorescence techniques in common sample preparations. Super-resolution microscopy

340 techniques such as *d*STORM and PALM have enabled new insights into how proteins are

341 organized in cells and multiprotein complexes, with a spatial resolution approaching virtually EM

342 level[2,3]. Nevertheless, structural details of the molecular architecture of multiprotein complexes

343 remained largely accessible only to EM methods. This inability of super-resolution microscopy

344 methods is often due to insufficient structural resolution, which is ultimately controlled by the

345 labeling density. Our results demonstrate that post-expansion labeling protocols substantially

346 increases the epitope accessibility for IgG antibodies resulting in higher labeling densities

347 especially of sterically demanding multiprotein complexes[14]. Consequently, MAP-SIM provides

348 improved ultrastructural resolution as demonstrated here for an important DNA-associated

349 multiprotein complex.

350

351

352

353

354

355

356

357

358

359

360

361

Online Methods

Animal care and experiments were conducted in accordance with the guidelines provided by the German Animal Welfare Act (German Ministry of Agriculture, Health and Economic Cooperation). Animal housing, breeding and were approved by the regulatory agency of the city of Wuerzburg (Reference 821-8760.00-10/90 approved 05.06.1992; according to §11/1 o.1 of the German Animal Welfare Act) and carried out following strict guidelines to ensure careful, consistent and ethical handling of mice.

Reagents

Acrylamide (AA, 40%, A4058, Sigma), Acryloyl-X, SE, 6-((acryloyl)amino)hexanoic Acid, Succinimidyl Ester (A20770, Thermo Fisher), Agarose (A9539, Sigma), Ammonium persulfate (APS, A3678, Sigma), Bovine Serum Albumin (BSA, A2153, Sigma), Dimethyl sulfoxide (DMSO, D12345, Thermo Fisher), Ethanol (absolute, ≥ 99.8%, 32205, Sigma), Ethylenediaminetetraacetic acid (EDTA, E1644, Sigma), Formaldehyde (FA, 36.5-38%, F8775, Sigma), Guanidine hydrochloride (guanidine HCl, 50933, Sigma), Glucose (G8270, Sigma), Glucoseoxidase (Sigma), ß-Mercaptoethylamine (MEA, M9768, Sigma), N,N'-methylen-bisacrylamide (BIS, 2%, M1533, Sigma), N,N,N′,N′-Tetramethylethylenediamine (TEMED, T7024, Sigma), Normal goat serum (50197Z, Thermo Fisher), PBS (P5493, Sigma), Poly-D-lysine hydropromide (P6407, Sigma), Polyoxyethylene (20) sorbitan monolaurate solution (Tween-20, 10%, 93774, Sigma), Potassium hydroxide (P1767, Sigma), Proteinase K (P4850, Sigma), Sodium acrylate (SA, 97-99%, 408220, Sigma), Sodium chloride (NaCl, S7653, Sigma), Sodium dodecyl sulfate (SDS, L3771, Sigma), Tris base (T6066, Sigma), Triton X-100 Surfact-Amps Detergent Solution (10% (w/v), 28313, Thermo Fisher), Tween 20 Surfact-Amps Detergent Solution (Tween-20, 28320, Sigma).

Murine spermatocyte cell spread preparation

Wildtype C57.6J/Bl6 mice were sacrificed using CO_2, followed by cervical dislocation. Testes were resected and seminiferous tubules extracted and immersed in PBS after decapsulation of the testes. Next, nuclear spreadings were carried out as described by de Boer et al.[46]. Briefly, seminiferous tubules were transferred to hypotonic buffer and incubated for 60 minutes. Individual seminiferous tubules were transferred to sterile sucrose solution on a slide, disrupted with forceps and cells flushed out by resuspension with a 10 µl pipette. In parallel, poly-lysine slides were immersed in 1% formaldehyde, substituted with acrylamide in case of the MAP and U-ExM protocol (30% AA, 4% FA in PBS for MAP and 1% AA, 0.7 % FA in PBS for U-ExM). 20

394   µl of the testes cells in sucrose were transferred to a drop of the formaldehyde solution collected

395   in a corner of the slide and spread evenly across the entire slide. Slides were incubated in a wet

396   chamber for 2 hours and dried overnight in a wet chamber left ajar. To ensure ease of handling,

397   nuclei were spread on round 18 mm coverslips (NO. 1.5H).

398   **Antibodies**

399   Guinea pig and rabbit anti-SYCP1 (N-terminal amino acids 1-124)[2], guinea pig anti-SYCP3 (N-

400   terminal amino acids 27-38) and rabbit anti-SYCE3 (full length protein) were generated by

401   Seqlab through immunizing the host with the respective peptides and affinity purified before use.

402   Rabbit anti-SYCP3 (NB300-232; derived against the C-terminus) was purchased from Novus

403   Biologicals and mouse anti-SYCP3 (ab97672; full length protein) was purchased from Abcam.

404   Al647 goat anti-guinea pig IgG (H+L), highly cross-absorbed (A-21450) Invitrogen

405   (ThermoFisher); goat anti-rabbit IgG (H+L) highly cross-adsorbed Alexa Fluor 568 (A-11036)

406   was purchased from ThermoFisher; Alexa 488 conjugated AffiPure F(ab')2 goat anti-guinea pig

407   IgG (H+L) was purchased from Dianova (106-546-003). SeTau647 NHS (K9-4149; SETA

408   Biomedicals) was conjugated to F(ab')2 of goat anti-mouse IgG (SA-10225; ThermoFisher);

409   F(ab')2 goat anti-rabbit IgG (H+L) cross-adsorbed Alexa Fluor 647 (A-21246) and F(ab')2 goat

410   anti-mouse IgG (H+L) cross-adsorbed Alexa Fluor 488 (A-11017) were purchased from

411   ThermoFisher. Supplementary Table 1 summarizes the immunolabeling used for the different

412   experiments.

413   **Immunofluorescence of non-expanded SCs**

414   Coverslips with fixated nuclear spreadings were washed with PBS. Unspecific epitopes were

415   blocked for 1 hour in 10 % NGS. Nuclear spreadings were incubated face down on 100 µl of the

416   primary antibody for 1 hour at room temperature in a humidified chamber. Spreadings were then

417   washed with PBS and blocked for 30 minutes in 10 % NGS before incubation with the secondary

418   antibody for 30 minutes at room temperature in a humidity chamber. For multi-color experiments,

419   immunostaining was performed sequentially, starting with the antibody raised in mouse.

420   **Protein retention protocol (proExM)**

421   *Gel linker treatment.* In order to cross-link amide groups into the polymeric hydrogel network,

422   samples were incubated in freshly prepared amine reactive AcX solution (0.1 mg/ml) in PBS.

423   Dessicated AcX stocks (10 mg/ml) stored as aliquots at -20°C were therefore resuspended in 10

424   µl anhydrous DMSO and diluted 1:100 in PBS (1x). Samples were then covered with 1 ml AcX

425   solution per coverslip and incubated at room temperature in a humidified chamber overnight.

426 *Gel formation, Digestion and Expansion.* Hydrogel formation was carried out on a cell culture
427 plate lid covered with parafilm. The plate was placed on ice to provide a cooled and flat
428 hydrophobic gelation surface. 80 µl of pre-chilled (4°C) gelling solution **(**8.55 % SA, 2.5% AA,
429 0.15 % Bis-AA, 0.2 % APS, 0.2% TEMED, 11.7% NaCl, 1x PBS) were prepared from proExM
430 Monomer stock solution consisting of a mixture of acrylic copolymers and crosslinking agent
431 (8.55 % SA, 2.5% AA, 0.15 % Bis-AA, 11.7% NaCl, 1x PBS) that was supplemented with radical
432 polymerization initiator APS and accelertator TEMED right before use. The gel solution was
433 placed on parafilm and coverslips were put on top of the formed droplet with spread cells facing
434 down. After 5min incubation on ice, crosslinking polymerization was allowed to occur for 1.5
435 hours at 37°C in a humidified chamber. Then samples were treated with 8 U /ml Proteinase K in
436 Digestion Buffer (50 mM Tris pH (8.0), 1 mM EDTA, 0.5 % Triton X-100, 0.8 M guanidine HCl).
437 For expansion of the samples, hydrogels were washed several times in double-deionized water
438 until the maximum extent of swelling of the gels was reached.

Magnified analysis of the proteome (MAP) and ultrastructure expansion microscopy (U-ExM) protocol

441 *Gel linker treatment.* In the case of MAP and U-ExM expanded samples, spreads were
442 incubated in AA/FA solution (30% AA, 4% FA in PBS for MAP and 1% AA, 0.7 % FA in PBS for
443 U-ExM) for 4 hours at 37°C in a humidified chamber before proceeding with gelation of the
444 samples.

445 *Gel formation, Denaturation and Expansion.* Following AA/FA incubation, samples were washed
446 three times for 5 minutes each in PBS (1x). Then polymerization of hydrogels was performed as
447 described under 'ProExM protocol' using an optimized MAP Gel solution (7 % SA, 20 % AA,
448 0.05 % Bis-AA, 0.5% APS, 0.5% TEMED, 1x PBS) or U-ExM Gel solution (19% SA, 10% AA,
449 0.1% BIS-AA, 0.5% APS, 0.5% TEMED, 1x PBS). The MAP monomer solution composition was
450 altered compared to the original recipe[7] regarding the monomer to crosslinking agent ratio. After
451 polymerization hydrogels were carefully removed from the coverslips and transferred directly into
452 pre-heated (95°C) Denaturation buffer (200 mM SDS, 200mM NaCl, 50 mM Tris, pH 9.0) in 1.5
453 ml centrifuge tubes. Samples were then denaturated for 1 hour in a heating block incubator with
454 closed tube lids. For swelling of the sample, hydrogels were washed with excess volume of
455 double-deionized water that was exchanged several times until the maximum expansion level
456 was reached.

Post-expansion immunolabeling of MAP and U-ExM treated samples

458   For MAP and U-ExM treated samples immunostaining was performed post expansion. Fully
459   expanded gels were incubated in Blocking buffer (0.15% BSA in PBS) twice for 30 minutes
460   each. Gels shrink during this blocking step. Then primary antibodies were incubated sequentially
461   for 3 hours each at 37°C in a humidified chamber with two 20 minutes washing steps in Blocking
462   buffer following each antibody incubation step. Next a secondary antibodies mix was added
463   simultaneously for 3 hours at 37°C in a humidified chamber. Samples were then washed twice
464   for 30 minutes each with Washing Buffer (0.1 % Tween-20 in PBS) and once more overnight.
465   Samples were then washed in double-deionized water and expanded back to the maximum
466   hydrogel volume.

Mounting of expanded samples

468   *Poly-Lysine coating of cover glasses.* 24 mm round cover glasses (NO. 1.5. H) were sonicated in
469   double-deionized water, 1 M KOH and absolute ethanol (≥ 99.8 %) for 15 minutes each.
470   Following each sonication step glasses were rinsed with double-deionized water. After
471   sonication glasses were finally dried at 100°C in an oven. Cover glasses were then covered with
472   0.1% Poly D-Lysine and incubated for 1 hour at room temperature. Next glasses were washed
473   again with water and air-dried and stored in a closed glass container to avoid dust
474   contamination. Coated coverslips were stored at 4°C and used for up to one week.

475   *Fluorescent Marker treatment of cover glasses.* Fluorescent beads introduced directly into the
476   hydrogel show strong fluorescence loss caused by persulfate radicals during polymerization. For
477   this reason we directly coated coverslips with fluorescent markers to perform channel alignment.
478   Therefore, fluorescent marker stock suspension (0.1 μm, ~1.8 × 10^{11} particles/mL, TetraSpeck
479   Microspheres, Thermo Fisher) was vortexed for ~1 minute and then diluted 1:1000 in PBS (1x)
480   and vortexed again briefly. Glasses were covered with the suspension for 30 minutes at room
481   temperature to let the fluorescent markers settle down. Then coverslips were washed with
482   double-deionized water, air-dried and thereupon used for hydrogel immobilization with Agarose.

483   *Agarose embedding.* Expanded samples were cut into ~1.5 x 1.5 cm pieces using a razor blade
484   and excess water was removed carefully from the gels with laboratory wipes. Gels were then
485   transferred onto Poly-Lysine coated coverslips. To further avoid drifting of the sample during
486   long-term image acquisition gels were additionally embedded in 1 % (w/v) Agarose in water.
487   Therefor a second uncoated round 18 mm-coverslip was placed on top of the cut hydrogel and
488   melted Agarose (~40°C) was carefully applied around the sides of the hydrogel using a pipette.
489   Care was taken to avoid Agarose from flowing below the hydrogel. The agarose gel was
490   subsequently hardened at 4°C for ~10 minutes and the upper coverslip was removed carefully.
491   Double deionized water was then added on the hydrogel to prevent dehydration during imaging.

Imaging

Structured Illumination Microscopy (SIM) imaging. SIM imaging was performed using a Zeiss Elyra S.1 SIM imaging system consisting of an inverse Axio Observer. Z1 microscope equipped with a C-APOCHROMAT 63x (NA 1.2) water-immersion objective and four different excitation lasers (405 nm diode, 488 nm OPSL, 561 nm OPSL and 642 nm diode laser). Three-dimensional SIM imaging of the expanded sample was recorded on a PCO edge sCMOS (scientific complementary metal-oxide semiconductor) camera with 0.110 μm z steps adjusted by an inserted Z-Piezo stage. Three rotations of the grid pattern were projected on the image plane for each acquired channel. The red fluorophore was imaged before fluorophores with lower wavelengths to minimize photobleaching. Raw data images were processed using the Zeiss ZEN software (black edition).

Channel alignment for SIM images. Fluorescent beads mounted on the coverslip that were localized directly below the sample imaging area were set as lowest imaging plane and recorded with the sample for each 3D z-stack. For alignment and SIM processing images containing fluorescent markers were cropped out and used to align the channels in each recorded z-stack via the Zeiss Zen software channel alignment tool.

Rescanning confocal microscopy (RCM) imaging. RCM imaging was conducted on a Nikon TiE inverted microscope combined with an RCM unit (Confocal.nl). RCM derives from the image-scanning principle whereby pixel reassignment is carried out purely optomechanically[31,47]. The unit is connected to a Cobolt Skyra (Cobolt, Hübner Group) laser unit providing four excitation laser lines (405 nm, 488 nm, 561 nm, and 640 nm). Images were recorded on an sCMOS camera (Zyla 4.2 P, Andor) using a 60x water-immersion objective (CFI Plan APO, 1.27-NA; Nikon) and a fixed 50 μm pinhole size. The setup was operated by the microscope software NIS-Elements (version 4.6).

d*STORM imaging. d*STORM acquisition of unexpanded samples were conducted on a home-built widefield imaging setup as described previously[20]. The setup consists of an inverted IX71 microscope (Olympus) equipped with an oil-immersion objective (APON 60XOTIRF, NA 1.49, Olympus). For excitation of Alexa Fluor 647, a 639 nm OPS laser diode (Genesis MX639-1000 STM; Coherent) was used in quasi-TIRF mode. To avoid drift during acquisition a nose-piece stage (IX2-NPS, Olympus) is implemented in the microscope. Fluorescence light was collected onto an electron-multiplying charge-couple device (EM-CCD) camera (iXon Ultra 897, Andor). As photoswitching buffer 100 mM ß-Mercaptoethylamine in PBS (pH 7.4) supplemented with 10 % (w/v) glucose and 0.5 mg/ml glucose oxidase as oxygen scavenger system was used. For image reconstruction the ImageJ plugin ThunderSTORM[48] was used.

Protein position analysis

SC cross-sectional profiles using 'Line Profiler'. The SYCE3 input image is convolved with a gaussian blur, compensating noise and intensity fluctuations. Via Otsu[47] thresholding the image is converted into a binary image. Using Lee's algorithm[7] a skeletonize image is constructed reducing all expanded shapes to lines with 1 pixel width. Subsequently all connected pixels unequal to zero were sorted und checked for continuity, i.e. sharp edges mark a breakpoint initiating a new line. The pixel coordinates of each line were fitted with a c-spline. The c-splines coordinates and local derivatives are a good estimation for the center and orientations of the helix structure SYCP3 channel. Note that the orientation and center of the SYCP3 channel can also be estimated with Sobel filters, if the SYCE3 channel cannot be evaluated ('1 channel' mode). To receive the areas of maximum distance, i.e. the areas where the SYCP3 helix structure is in plane, a floodfill algorithm and a distance transform[8], with a subsequent thresholding to 40 % of the maximum value, were applied. Using a logical and operation on the line coordinates and the thresholded distance transform image resulted in the desired source coordinates and directions for further evaluation. Line profiles were then constructed originating at the source coordinates perpendicular to the c-splines derivative or respectively in Sobel gradient direction at the edge points of the SYCP3 channel. The line profiles were post aligned at the center of the two global maxima. Average profiles were returned for each line and for the whole image.

Protein distribution of SYCE3 and SYCP1N. To determine the distribution of SYCE3, areas of the SYCE3 signal were manually chosen from regions where SYCP3 strands showed a helix crossing. These regions can be regarded as frontal views of the SYCE3 and SYCP1N proteins and were used for cross-sectional profiling (**Fig 4**).

Expansion factor determination. The expansion factor was determined by dividing the distances of the two SYCP3 strands measured from expanded SIM and unexpanded *d*STORM measurements. Here, strand distances of unexpanded SCs visualized by *d*STORM were determined using the `Line Profiler` with Sobel filter settings for '1 channel' analysis as described above and shown in **Supplementary Fig. 3**. Although the analysis of expanded MAP-SIM and U-ExM SIM data are possible using the SYCE3 channel to determine SC orientation, for reasons of comparability the expanded strand distance values were determined in the same '1-channel mode' Line Profiler settings as for unexpanded *d*STORM analysis. Note that the '2-channel mode' also includes areas which are closer to the SYCP3 strand crossings in comparison to the '1-channel mode' (compare **Supplementary Fig. 1** and **Supplementary Fig. 2**). The expansion

559 factor was then calculated by dividing the resulting mean values of expanded SYCP3 distances

560 with the distance mean value of unexpanded *d*STORM data.

561 *3D visualization of MAP-SIM data.* 3D MAP SIM data shown in **Supplementary Video 1** and

562 **Supplementary Video 2** were visualized using the microscopy image analysis software IMARIS

563 (version 8.4.1, Bitplane).

564 *Averaging of cross-sectional profiles.* The resulting cross-sectional profiles were finally averaged

565 using the data analysis software Origin(Pro) Version 2016.

566 **References**

567 1. Koster, A. J. & Klumperman, J. Electron microscopy in cell biology: integrating structure and
568   function. *Nat. Rev. Mol. Cell Biol.* **Suppl.** SS6-10 (2003).

569 2. Sauer, M. & Heilemann, M. Single-molecule localization microscopy in eukaryotes. *Chem.
570   Rev.* **117**, 7478-7509 (2017).

571 3. Schermelleh, L. *et al.* Super-resolution microscopy demystified. *Nat. Cell Biol.* **21**, 72-84
572   (2019).

573 4. Chen, F., Tillberg, P. W. & Boyden, E. S. Optical imaging expansion microscopy. *Science*
574   **347**, 543–548 (2015).

575 5. Chozinski, T. J. *et al.* Expansion microscopy with conventional antibodies and fluorescent
576   proteins. *Nat. Methods* **13**, 485–488 (2016).

577 6. Tillberg, P. W. *et al.* Protein-retention expansion microscopy of cells and tissues labeled
578   using standard fluorescent proteins and antibodies. *Nat. Biotechnol.* **34**, 987–992 (2016).

579 7. Ku, T. *et al.* Multiplexed and scalable super-resolution imaging of three-dimensional protein
580   localization in size-adjustable tissues. *Nat. Biotechnol.* **34**, 973–981 (2016).

581 8. Chen, F. *et al.* Nanoscale imaging of RNA with expansion microscopy. *Nat. Methods* **13**,
582   679–684 (2016).

583 9. Cahoon, C. K. *et al.* Superresolution expansion microscopy reveals the three-dimensional
584   organization of the Drosophila synaptonemal complex. *Proc. Natl. Acad. Sci. USA* **114**,
585   E6857-E6866 (2017).

586 10. Gao, M. *et al.* Expansion stimulated emission depletion microscopy (ExSTED). *ASC Nano*
587   **12**, 4178-4185 (2018).

588 11. Kunz, T.C., Götz, R., Sauer, M. & Rudel, T. Detection of Chlamydia developmental forms
589   and secreted effectors by expansion microscopy. *Front. Cell. Infect. Microbiol.* **9**, 276 (2019).

590 12. Truckenbrodt, S., Maidorn, M., Crzan, D., Widhagen, H., Kabatas, S. & Rizzoli, S. O. X10
591   expansion microscopy enables 25-nm resolution on conventional microscopes. *EMBO Rep.*
592   e45836 (2018).

13. Chang, J. B. *et al.* Iterative expansion microscopy. *Nat. Methods* **14**, 593–599 (2017).

14. Gambarotto, D. *et al.* Imaging cellular ultrastructures using expansion microscopy (U-ExM). *Nat. Methods* **16**, 71-74 (2019).

15. Moses, M. J. (1968). Synaptonemal complex. *Annual review of genetics* **2**, 363-412.

16. Sotelo, J. R. (1969). Ultrastructure of the chromosomes in meiosis. In: Handbook of Molecular Cytology, Ed. Lima de Faria A, pp 412-434; 1969, North Holland Pub. Co. Amsterdam.

17. Westergaard, M., & von Wettstein, D. (1972). The synaptonemal complex. *Annu. Rev. Genet.* **6**, 71-110.

18. Schmekel, K., & Daneholt, B. (1995). The central region of the synaptonemal complex revealed in three dimensions. *Trends in cell biology* **5**, 239-242.

19. Hernández-Hernández, A., Masich, S., Fukuda, T., Kouznetsova, A., Sandin, S., Daneholt, B., & Höög, C. (2016). The central element of the synaptonemal complex in mice is organized as a bilayered junction structure. *J. Cell Sci* **129**, 2239-2249.

20. Schücker, K., Holm, T., Franke, C., Sauer, M. & Benavente, R. Elucidation of synaptonemal complex organization by super-resolution imaging with isotropic resolution. *Proc. Natl. Acad. Sci. USA* **112**, 2029–2033 (2015).

21. Cahoon, C. K., Yu, Z., Wang, Y., Guo, F., Unruh, J. R., Slaughter, B. D., & Hawley, R. S. (2017). Superresolution expansion microscopy reveals the three-dimensional organization of the Drosophila synaptonemal complex. *Proceedings of the National Academy of Sciences* **114**, E6857-E6866.

22. Wang, Y. *et al.* Combined expansion microscopy with structured illumination microscopy for analyzing protein complexes. *Nat. Protocols* **13**, 1869–1895 (2018).

23. Xu, H. *et al.* Molecular organization of mammalian meiotic chromosome axis revealed by expansion STORM microscopy. *Proc. Natl. Acad. Sci. USA* **116**, 18423-18428 (2019).

24. Fraune, J., Schramm, S., Alsheimer, M. & Benavente, R. The mammalian synaptonemal complex: protein components, assembly and role in meiotic recombination. *Exp. Cell Res.* **318,** 1340-1346 (2012).

25. Bolcun-Filas, E. & Handel, M.A. Meiosis: the chromosomal foundation of reproduction. *Biol. Reprod.* **99,** 112-126 (2018).

26. Zwettler, F. et al. (2019) Synaptonemal Complex Line Profiler. 10.5281/zenodo.2643214 https://doi.org/10.5281/zenodo.2643214

27. Laemmli, U. K. (1970). Cleavage of structural proteins during the assembly of the head of bacteriophage T4. *Nature* **227**, 680.

627 28. Ninfa, A. J., & Ballou, D. P. (1998). *Fundamental laboratory approaches for biochemistry and*
628   *biotechnology* (pp. 247-271). Bethesda, MD: Fitzgerald Science Press.

629 29. van de Linde, S. *et al.* (2011) Direct stochastic optical reconstruction microscopy with
630   standard fluorescent probes. *Nat. Protocols* **6**, 991-1009.

631 30. Dempsey, G. T., Vaughan, J. C., Chen, K. H., Bates, M., & Zhuang, X. (2011). Evaluation of
632   fluorophores for optimal performance in localization-based super-resolution imaging. *Nature*
633   *Methods* **8**, 1027.

634 31. De Luca, G.M.R., Greedijk, R.M.P., Brandt, R.A.J., Zellenberg, C.H.C., de Jong, B.E.,
635   Timmermanns, W., Azar, L.N., Hoebe, R.A., Stallinga, S. & Manders, E.M.M. (2013) Re-scan
636   confocal microscopy: scanning twice for better resolution. *Biomed. Opt. Express* **4**, 2644-
637   2656.

638 32. Schmekel, K., Wahrman, J., Skoglund, U., & Daneholt, B. (1993a). The central region of the
639   synaptonemal complex in Blaps cribrosa studied by electron microscope tomography.
640   *Chromosoma* **102**, 669-681.

641 33. Schmekel, K., Skoglund, U., & Daneholt, B. (1993b). The three-dimensional structure of the
642   central region in a synaptonemal complex: a comparison between rat and two insect
643   species, Drosophila melanogaster and Blaps cribrosa. *Chromosoma* **10***2*, 682-692.

644 34. Spindler, MC. et al. (2019). Quantitative basis of meiotic chromosome synapsis analyzed by
645   electron tomography. *BioRxiv* [Preprint]. Available at https://doi.org/10.1101/705764.

646 35. Comings, D. E., & Okada, T. A. (1971). Fine structure of the synaptonemal complex: Regular
647   and stereo electron microscopy of deoxyribonuclease-treated whole mount preparations.
648   *Experimental cell research* **65**, 104-116.

649 36. Counce, S. J., & Meyer, G. F. (1973). Differentiation of the synaptonemal complex and the
650   kinetochore in Locusta spermatocytes studied by whole mount electron microscopy.
651   *Chromosoma* 44, 231-253.

652 37. Wahrman, J. (1981). Synaptonemal complexes-Origin and Fate. *Chromosomes today* **7**,
653   105-113.

654 38. Heyting, C., Dietrich, A. J., Redeker, E. J. W., & Vink, A. C. (1985). Structure and
655   composition of synaptonemal complexes, isolated from rat spermatocytes. *European journal*
656   *of cell biology*, **36**, 307-314.

657 39. Dresser, M. E., & Moses, M. J. (1980). Synaptonemal complex karyotyping in spermatocytes
658   of the Chinese hamster (Cricetulus griseus). *Chromosoma* **76**, 1-22.

659 40. Nebel, B. R., & Coulon, E. M. (1962). The fine structure of chromosomes in pigeon
660   spermatocytes. *Chromosoma* **13**, 272-291.

41. Del Mazo, J., & Gil-Alberdi, L. G. (1986). Multistranded organization of the lateral elements of the synaptonemal complex in the rat and mouse. *Cytogenetic and Genome Research* **41**, 219-224.

42. Solari, A. J. (1993). *Sex chromosomes and sex determination in vertebrates.* CRC Press.

43. Sciurano, R. B., De Luca, G., Rahn, I. M., & Solari, A. J. (2017). The XY Body of the Cat (Felis catus): Structural Differentiations and Protein Immunolocalization. *Cytogenetic and genome research* **152**, 137-147.

44. Syrjänen, J. L., Pellegrini, L., & Davies, O. R. (2014). A molecular model for the role of SYCP3 in meiotic chromosome organisation. *Elife* **3**, e02963.

45. Franco, M. J., Sciurano, R. B., & Solari, A. J. (2007). Protein immunolocalization supports the presence of identical mechanisms of XY body formation in eutherians and marsupials. *Chromosome research* **15**, 815-824.

46. de Boer, E., Lhuissier, F. G., & Heyting, C. (2009). Cytological analysis of interference in mouse meiosis. In *Meiosis* (pp. 355-382). Humana Press, Totowa, NJ.

47. Luca, G. M. R. de *et al.* (2017) Configurations of the Re-scan Confocal Microscope (RCM) for biomedical applications. *Journal Microsc.* **266,** 166–177).

48. Ovesný, M., Křížek, P., Borkovec, J., Švindrych, Z. & Hagen, G. M. (2014) ThunderSTORM: a comprehensive ImageJ plug-in for PALM and STORM data analysis and super-resolution imaging. *Bioinformatics* **30,** 2389–2390.

Acknowledgements

Author contributions

F.U.Z., M.C.S., M.S., and R.B. conceived and designed the project. M.S and R.B. supervised the project. F.U.Z, M.C.S., A.K. and T.K performed all experiments. S.R. developed Line profiler. S.R. and F.U.Z. performed data analysis. All authors wrote and revised the final manuscript.

694 **Additional information**

695 Supplementary information accompanies this paper at …….

696 **Ethics statement**

697 Animal care and experiments were conducted in accordance with the guidelines provided by the

698 German Animal Welfare Act (German Ministry of Agriculture, Health and Economic

699 Cooperation). Animal housing, breeding and experimental protocols were approved by the

700 regulatory agency of the city of Wuerzburg (Reference 821-8760.00-10/90; according to §11/1

701 No.1 of the German Animal Welfare Act) and carried out following strict guidelines to ensure

702 careful, consistent and ethical handling of mice.

703 **Competing interests:** The authors declare no competing interests.

704

705 **Figures**
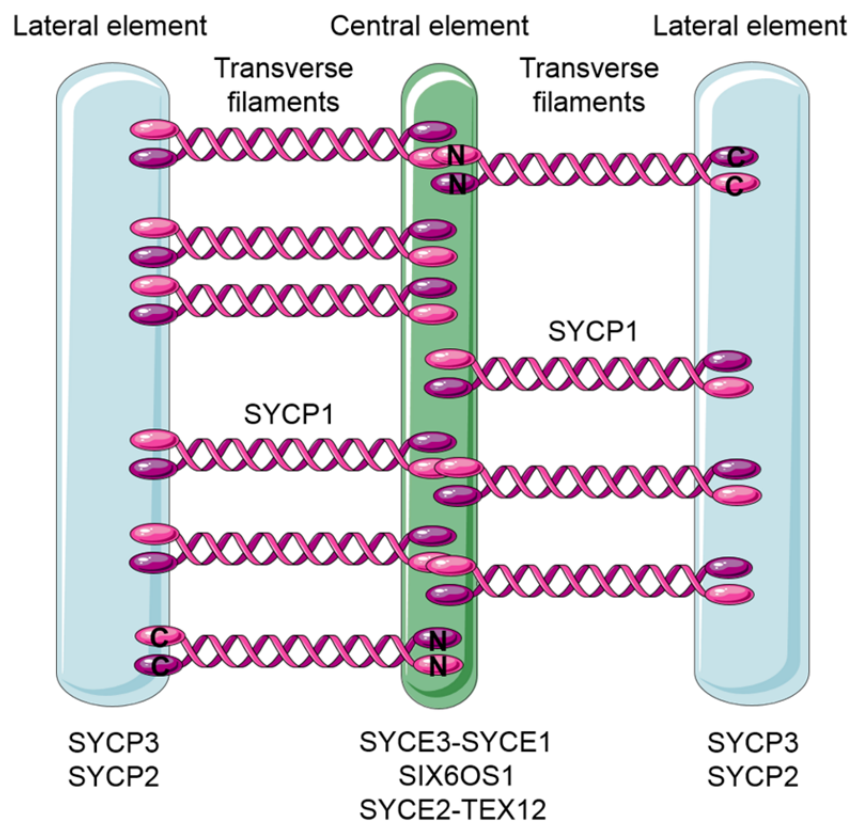
706

707 **Figure 1. The synaptonemal complex.** Schematic representation of the tripartite SC structure
708 showing the two lateral elements (LEs) consisting of SYCP2 and SYCP3 flanking the central
709 element comprised of SYCE1/2/3, Tex 12 and SIX6OS1. The transverse filament protein SYCP1
710 is connecting the lateral element and the central element with the SYCP1 C-terminus residing in
711 the lateral and the N-terminus in the central element[34].

712

713

714

715

716
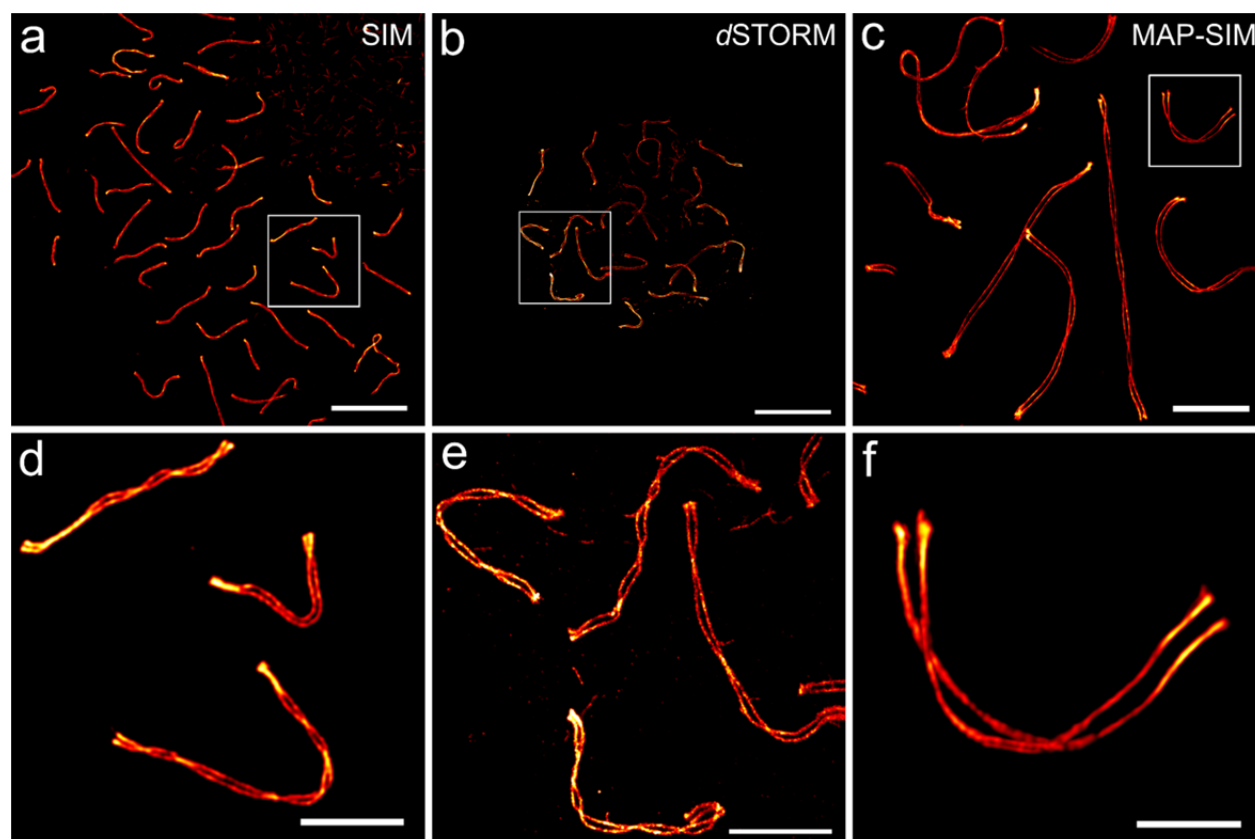
Figure 2. Super-resolution imaging of the lateral element protein SYCP3. a, SIM image of unexpanded SYCP3 labeled with Alexa Fluor 568. **b,** *d*STORM image of unexpanded SYCP3 labeled with Alexa Fluor 647. **c,** Expanded MAP-SIM SYCP3 signal (maximum intensity projection) labeled with SeTau-647. **d-f,** Magnified views of boxed regions in (**a**), (**b**) and (**c**), respectively. The images indicate that MAP-SIM provides a similar labeling density and spatial resolution as *d*STORM of 20-30 nm in the imaging plane. Scale bars. (**a**-**c**) 10 μm. (**d**-**f**) 3 μm.

724

725

726

727

728

729

730
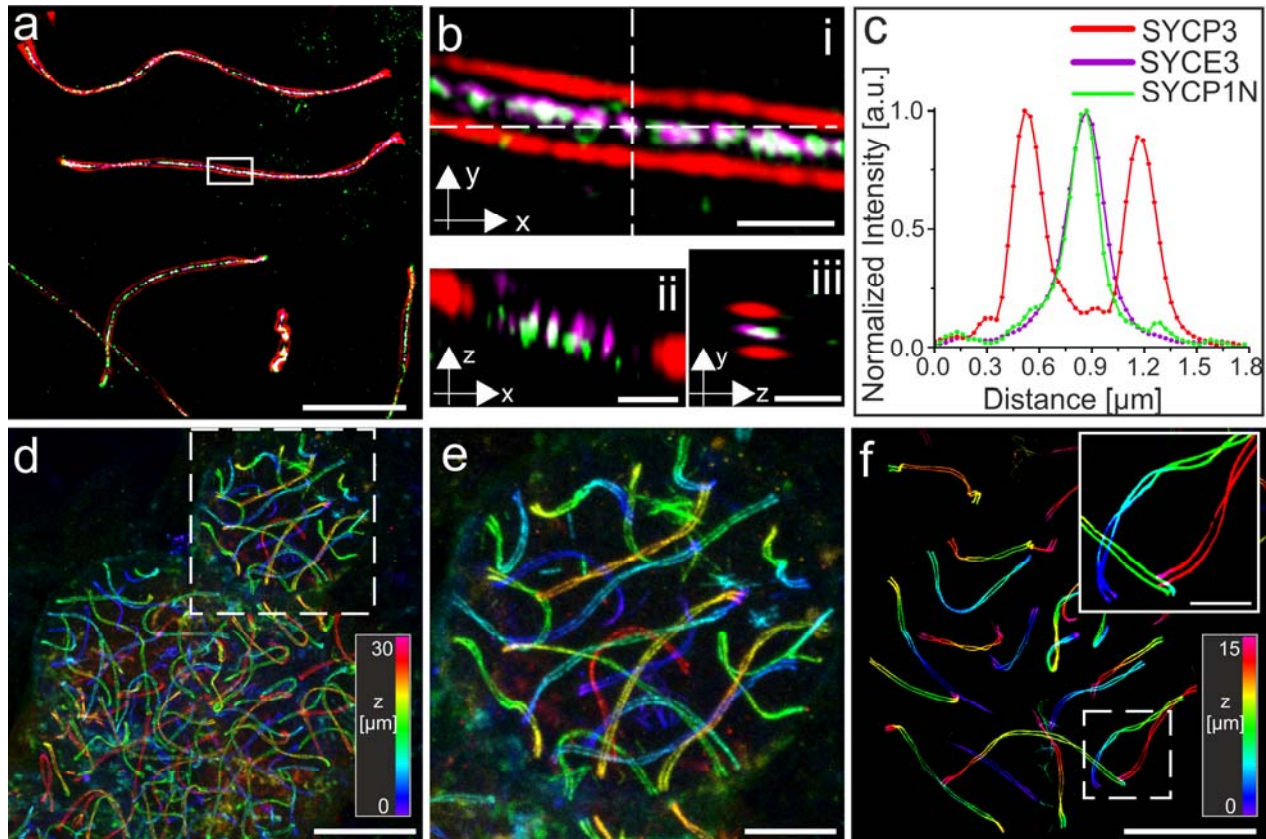
Figure 3. 3D-Multicolor MAP-SIM of SYCP3, SYCP1 N-terminus, and SYCE3. a, SIM image of post-expansion SeTau-647 labeled SYCP3 as a component of the lateral element (red), the transverse filament SYCP1 N-terminus labeled with Alexa Fluor 488 (green) and SYCE3 of the central element labeled with Alexa Fluor 568 (magenta). **b,** Magnified views of white boxed region in (**a**). **ii,** Orthogonal view of horizontal white dashed line in (i). **iii,** Orthogonal view of vertical white dashed line in (i). **c,** Transversal intensity profile perpendicular to the orientation of the SC shown in (**b**). The selected section exhibits a bimodal distribution of the SYCP3 signal separated by 667.0 nm ± 7.1 nm. The SYCP1 N-terminus and SYCE3 signals of the section (b) show monomodal distributions with FWHM of 214.7 ± 6.9 nm and 258.3 ± 4.8 nm, respectively. **d**, Large field of view (100x100x30 µm³) 3D-Re-scan confocal microscopy image of spreaded cells. SYCP3 was labeled post-expansion with SeTau-647. **e,** Magnified view of boxed region in (d). **g,** 3D-MAP-SIM image of the SCs of an entire set of chromosomes in a spermatocyte visualized by post-expansion labeling of SYCP3 with SeTau-647. The inlet shows the enlarged view of the boxed region in (**f**). Scale bars. (**a**) 10 µm. (**b-d**) 1 µm. (**f**) 10 µm. (**g**) 15 µm. (**h**) 5 µm.
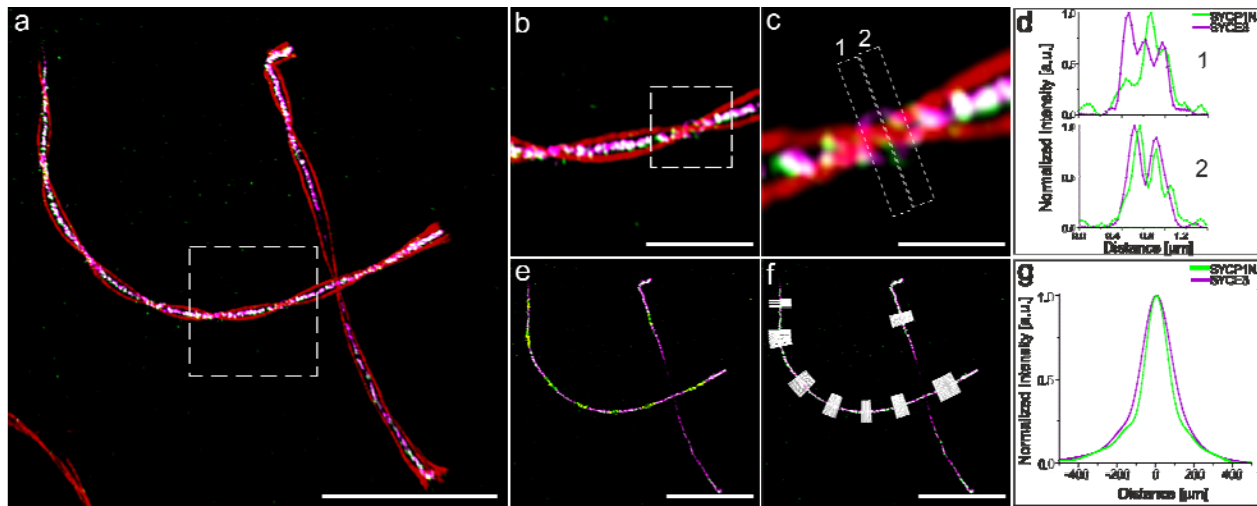
746

747

748

749

750

751

752

753

754

Figure 4. Protein distribution of the SYCP1 N-terminus reveals complex network organization of the SC central region. a, Lateral view MAP-SIM image of SYCE3 labeled with Alexa Fluor 568 (magenta), SYCP1N labeled with Alexa Fluor 488 (green) and SYCP3 labeled with SeTau-647 (red). Regions where the SC twists as visualized by the twisting SYCP3 signal (lateral view) show partially a multimodal organization of the N-terminus of the transverse filament protein SYCP1 and the central element protein SYCE3. **b,** Magnified view of white boxed region in (**a**). **c,** Enlarged view of highlighted region in (**b**) with two sites selected for protein distribution analysis (1, 2). **d,** Respective cross-sectional intensity profiles along SYCE3 and SYCP1N of the regions specified in (**c**). **e,** SYCE3 and SYCP1N signals as in (**a**) without SYCP3 signal. Frontal views of the two proteins used for cross-sectional profiles are shown in yellow. **f,** as in (**e**) with line profiles (white) perpendicular to the frontal view of the SYCE3 signal. **g,** Averaged intensity line profile of all profiles shown in (**f**) with a monomodal signal distribution of 168.0 ± 1.1 nm (SD) for SYCP1N and 211.43 ± 0.89 nm for SYCE3 derived from single Gaussian fitting. Scale bars, (**a**) 10 µm, (**b**) 3µm, (**c**) 1 µm, (**e**-**f**) 10µm.
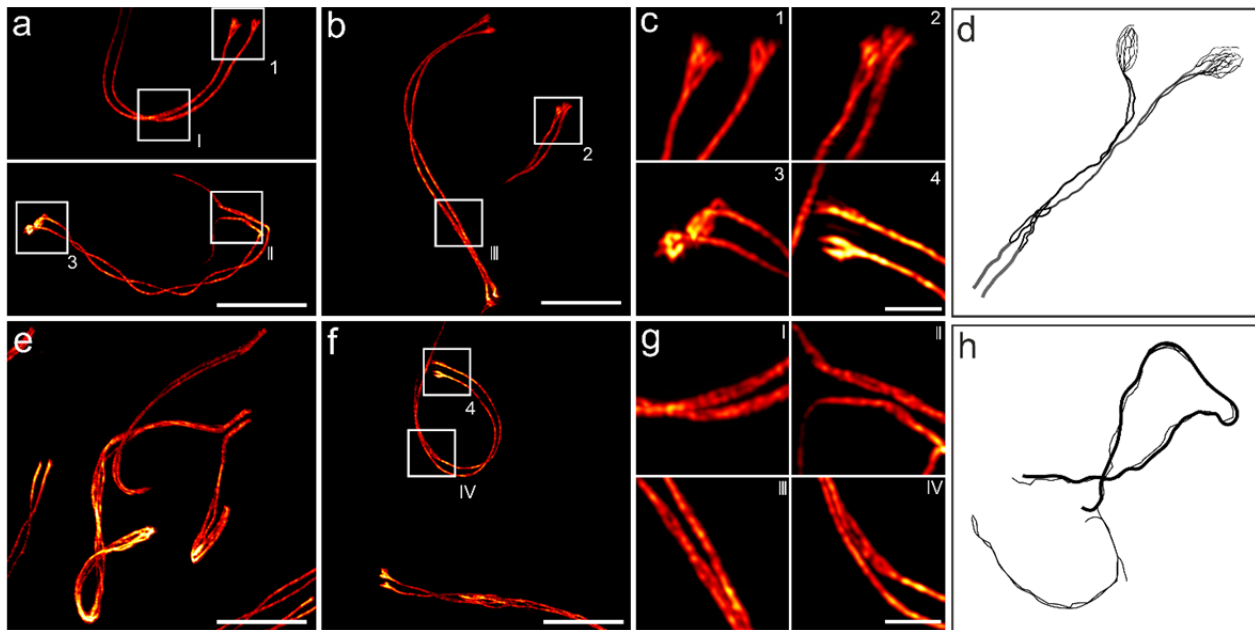
769

770

771

772

773

774

775

776

777

778

779

780

781
782

Figure 5. Structural details of the SC lateral element revealed by MAP-SIM of SYCP3. a-c, f, g, The SYCP3 signal shows occasional bifurcation along the two SC strands (I-IV) and various degrees of fraying at their ends depending on the respective pachytene stage (1-4). **e,** Unpaired regions of the XY pair also show a strong degree of fraying. **d, h,** Schematic representations of early EM reports of two or more sub lateral elements (subLEs) in mammals[38,40] in accordance with the splitting of the SYCP3 signal resolved by MAP-SIM in this study. **d,** Representation of the lateral element strand splitting in two and fraying at its end according to Figure 4b and 3a of del Mazo and Gil-Alberdi, 1986[38]. **h,** Fraying of LEs associated with unpaired regions of the XY pair modelled after Figure 10c of Dresser and Moses, 1980[40]. Scale bars, (**a-b**) 7 μm, (**c**) 1.5μm, (**e-f)** 7 μm, (**g**) 1.5μm.

793
794

795

796

797

798

799

800

801

802

803

804

Supplementary Figures

806

807

Tracking down the molecular architecture of
the synaptonemal complex by expansion microscopy

810

811

Fabian U. Zwettler[#1], Marie-Christin Spindler[#2], Sebastian Reinhard[1], Teresa Klein[1],

Andreas Kurz[1], Markus Sauer*[1], and Ricardo Benavente*[2]

814

815
816
817

[1]Department of Biotechnology and Biophysics, Biocenter, University of Würzburg,

Am Hubland, 97074 Würzburg, Germany

820

[2]Department of Cell and Developmental Biology, Biocenter, University of Würzburg,

Am Hubland, 97074 Würzburg, Germany

823

824

[#]These authors contributed equally to this work

826

Correspondence and requests for materials should be addressed to M.S. and R.B. (m.sauer@uni-wuerzburg.de and benavente@biozentrum.uni-wuerzburg.de)

829
830

831

	Primary antibodies	Secondary antibodies	Figures
*d*STORM	SYCP3 (guinea pig)	Al647 goat anti guinea pig	Fig.2b,2e; S.Fig. 3
Unexpanded SIM	SYCP3 (rabbit)	Al568 goat anti rabbit	Fig.2a, 2d
MAP-SIM MAP-RCM	SYCP3 (mouse) SYCE3 (rabbit) SYCP1N (guinea pig)	SeTau647 goat anti mouse Al568 goat anti rabbit Al488 goat anti guinea pig	Fig.2c,2f; Fig.3; Fig.4; Fig. 5; S.Fig 1; S.Fig 2
U-ExM SIM	SYCP3 (mouse) SYCE3 (rabbit) SYCP1N (guinea pig)	SeTau647 goat anti mouse Al568 goat anti rabbit Al488 goat anti guinea pig	S.Fig 4a-c

832

833   **Supplementary Table 1: Immunolabeling used in the different experiments**

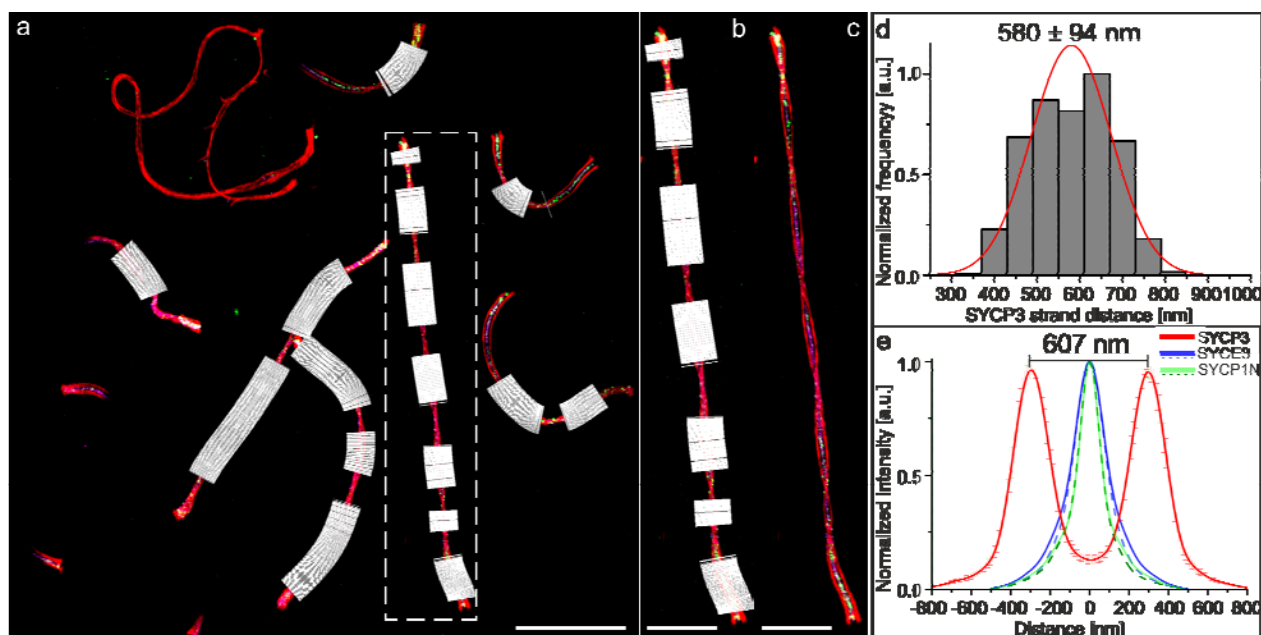| **Pro-ExM** | SYCP3 (mouse) | AI488 goat anti mouse | S.Fig 4d-f |
| | SYCP1N (rabbit) | AI647 goat anti rabbit | |

834

835

836

837

838

839

840

841

842
843
844 **Supplementary Figure 1**. **2-channel-mode. a**, Three-color-SIM image (maximum intensity
845 projection) with line profiles (white) oriented along the SC at regions where SYCP3 shows a
846 bimodal signal distribution using SYCE3 as criterion for the center of the SC. SYCP3 labeled
847 with SeTau647 (red), SYCP1N labeled with Alexa Fluor 488 (green) and SYCE3 labeled with
848 Alexa Fluor 568 (magenta). **b**, Magnified view of white dashed box in (**a**). **c**, Same as (**b**) without
849 line profiles. **d**, Histogram of SYCP3 distances of 17,607 line profiles determined from 97 MAP-
850 SIM expanded and imaged SCs from two separate experiments. The SYCP3 distance has been
851 determined to 580 ± 93 nm (SD). **e**, Averaged intensity profiles of SYCP3 (red), SYCE3 (blue)
852 and SYCP1N (green) of all analyzed MAP-SIM data in (**d**). Dashed curves show the averaged
853 protein distribution of line profiles only set at frontal views of SYCP3. Whereas solid lines are
854 from data along the complete SC including areas where SYCP3 shows a helical crossing. Fitting
855 of the SYCP3 distribution with a bimodal Gaussian function resulted in a peak-to-peak distance

856 of 607 nm. SYCP1N and SYCE3 showed a monomodal protein distribution of 161.5 ± 1.3 nm
857 (FWHM) for SYCP1N and 229.3 ± 1.2 nm (FWHM) for SYCE3 including SYCP3 crossing point
858 areas. Analysis of the protein distributions without SYCP3 crossing point areas resulted in
859 FWHM of 160.2 ± 1.1 nm for SYCP1N and 207.5 ± 0.78 nm for SYCE3. Scale bar. (**a**) 10 µm.
860 (**b-c**) 5µm.

861
862
863
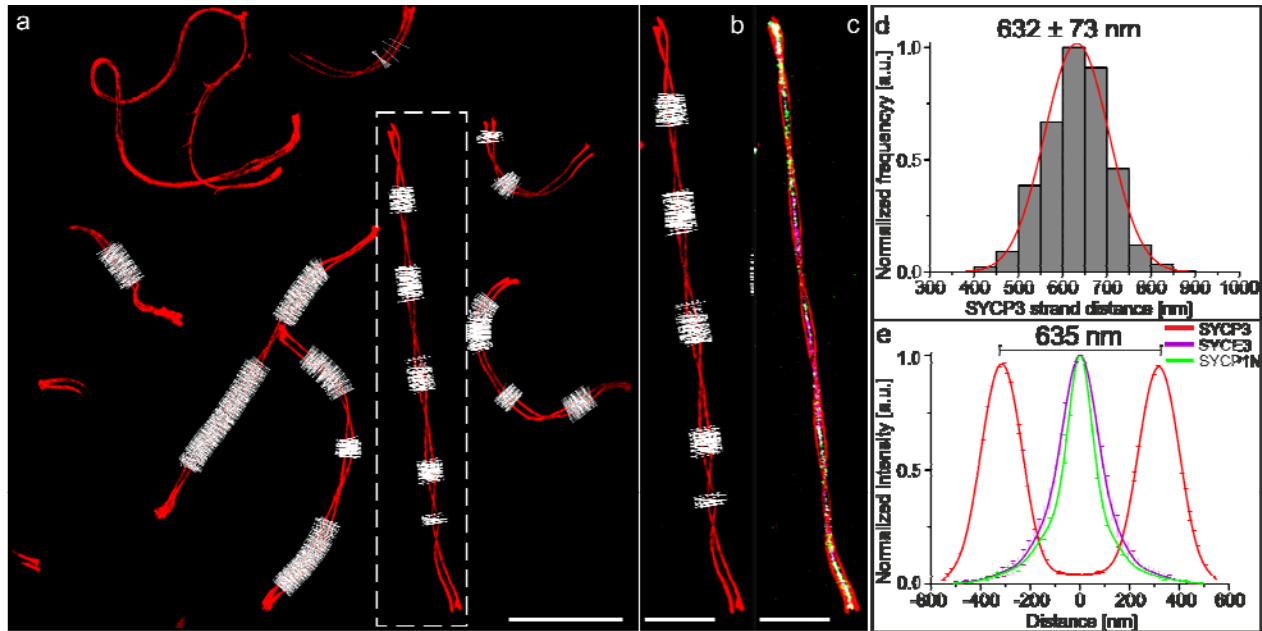
864
865
866 **Supplementary Figure 2**. **1-channel mode**. **a**, Same three-color-SIM image (maximum
867 intensity projection) as shown in **Supplementary Fig. 1** but with line profiles (white) oriented
868 along the SC with SYCP3 (red) as criterion for the center of the SC. Profiles are set at regions
869 where a bimodal signal distribution of the protein is occurring. **b**, Magnified view of white dashed
870 box in (**a**). **c**, Same as (**b**) with SYCP1N (green) and SYCE3 (magenta) without cross-sectional
871 profiles. **d**, Histogram of SYCP3 distances of 18,136 line profiles determined from the same data
872 set analyzed in **Supplementary Fig. 1**. The SYCP3 distance has been determined to 632 ± 73
873 nm (SD). Note that different values of the strand distances compared to **Supplementary Fig. 1c**
874 occur from areas that are not detected for line profiling that are closer to helical crossing overs
875 when using SYCP3 to determine the center of the SC. **e**, Averaged intensity profiles of SYCP3
876 (red), SYCP1 N (green) and SYCE3 (magenta) of the analyzed MAP-SIM data in (**d**). Fitting of
877 the SYCP3 distribution with a bimodal Gaussian function results in a peak-to-peak distance of
878 635 nm. Scale bar. (**a**) 10 µm. (**b-c**) 5 µm.

879
880
881
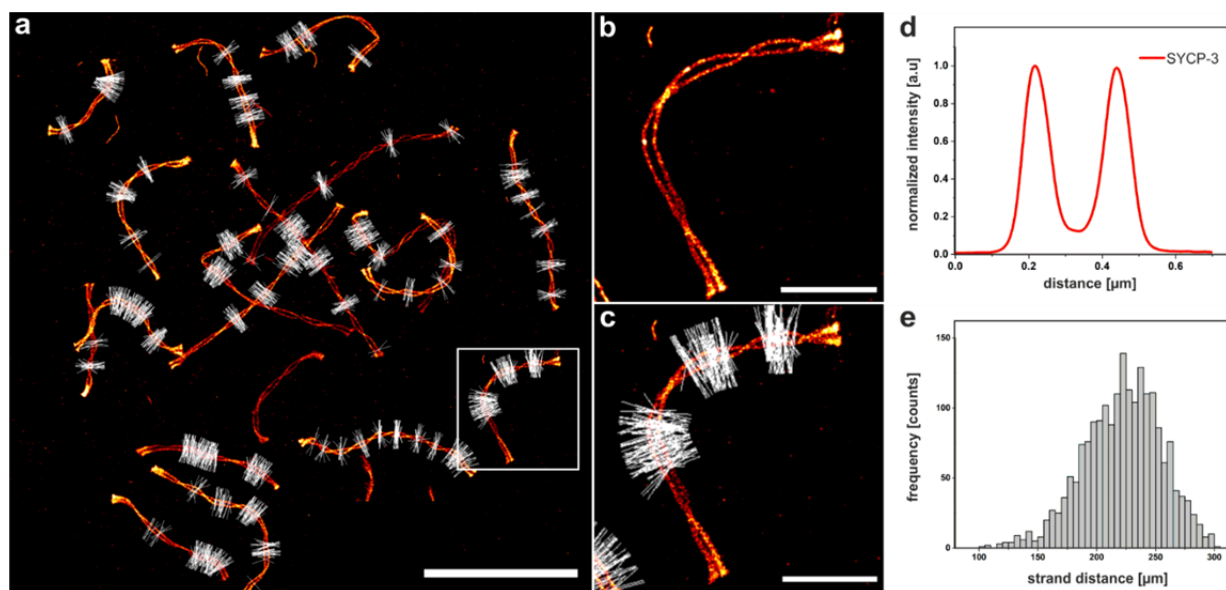
882
883

884 **Supplementary Figure 3**. **a**, *d*STORM image of unexpanded SYCP3 labeled with Alexa Fluor
885 647 (red) with intensity line profiles (white) along the SC using SYCP3 to define the center and
886 orientation of the complexes. **b,** Enlarged view of white box highlighted in (a) without line
887 profiles. **c,** Same as (b) with line profiles (white) along the SYCP3 signal. **d,** Averaged intensity
888 line profile of all profiles shown in (a). A bimodal Gaussian fit of the protein positions gives a
889 peak-to-peak distance of 230 nm (SD). **e,** Histogram of SYCP3 strand distances resulting from
890 line profiles shown in (a) with a mean value of 222 ± 33 nm (SD). Scale bars, (**a**) 10μm, (**b-c**)
891 2μm.

892
893
894
895
896
897
898
899
900
901
902
903
904
905
906
907
908
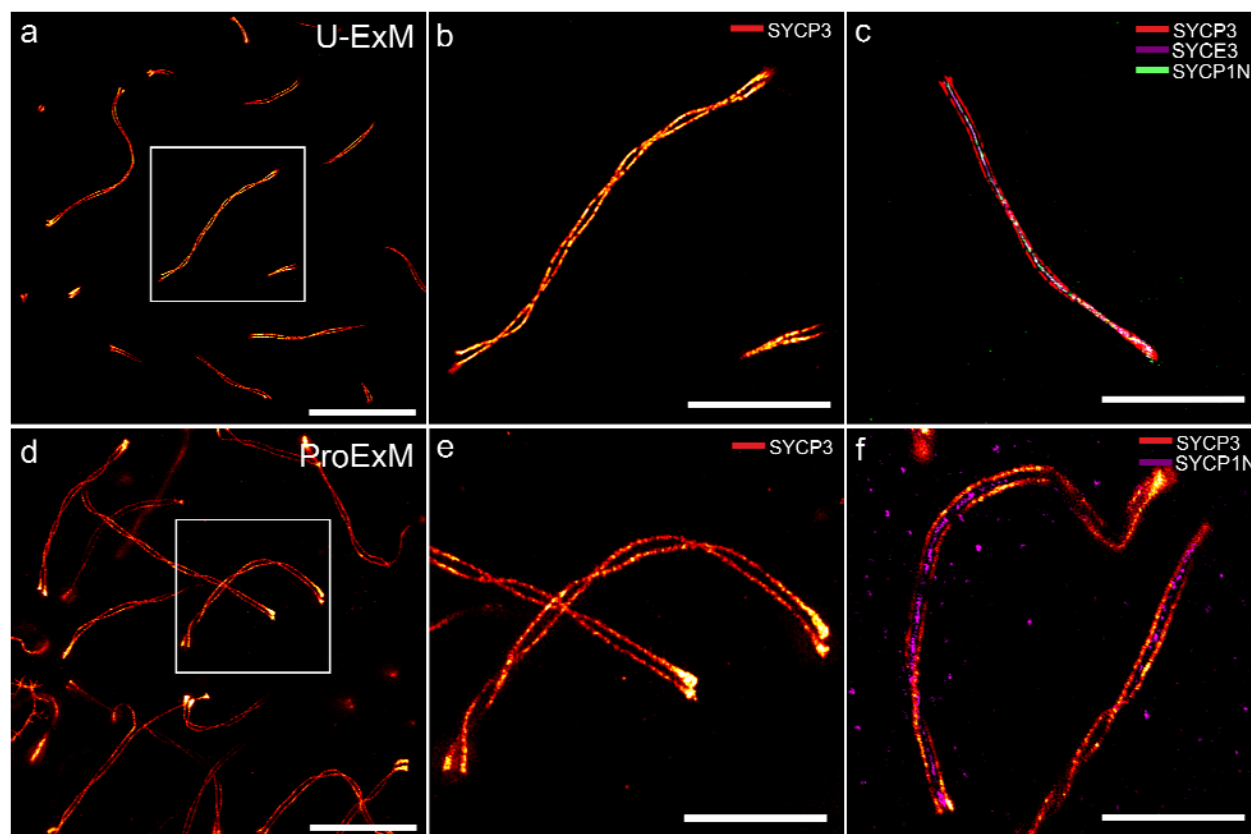
909
910
911 **Supplementary Figure 4**. **a**, SIM image (maximum intensity projection of a z-stack) of U-ExM
912 expanded SCs, post-expansion labeled for SYCP3 by immunolabeling with SeTau647. **b**,
913 Magnified view of boxed region in (**a**). **c**, Maximum intensity projection of a z-stack of a
914 multicolor SIM image of an U-ExM expanded SC post-expansion labeled with SeTau647 for
915 SYCP3 (red), SYCE3 labeled with labeled with Alexa Fluor 568 (magenta), and SYCP1N labeled
916 with Alexa Fluor 488 (green). **d**, SIM image (maximum intensity projection of a z-stack) of
917 proExM expanded SCs, pre-expansion labeled for SYCP3 by immunolabeling with Alexa Fluor
918 488. **e**, Magnified view of boxed region in (**d**). **f**, Maximum intensity projection of a z-stack of a
919 two-color SIM image of a proExM expanded SC pre-expansion labeled with Alexa Fluor 488 for
920 SYCP3 (red) and SYCP1N labeled with labeled with Alexa Fluor 647 (magenta). Scale bars. (**a**)
921 20 µm, (**b-c**) 10 µm, (**d**) 20 µm, (**e-f**) 10 µm.
922
923
924
925
926
927
928
929
930
931
932
933
934
935
936
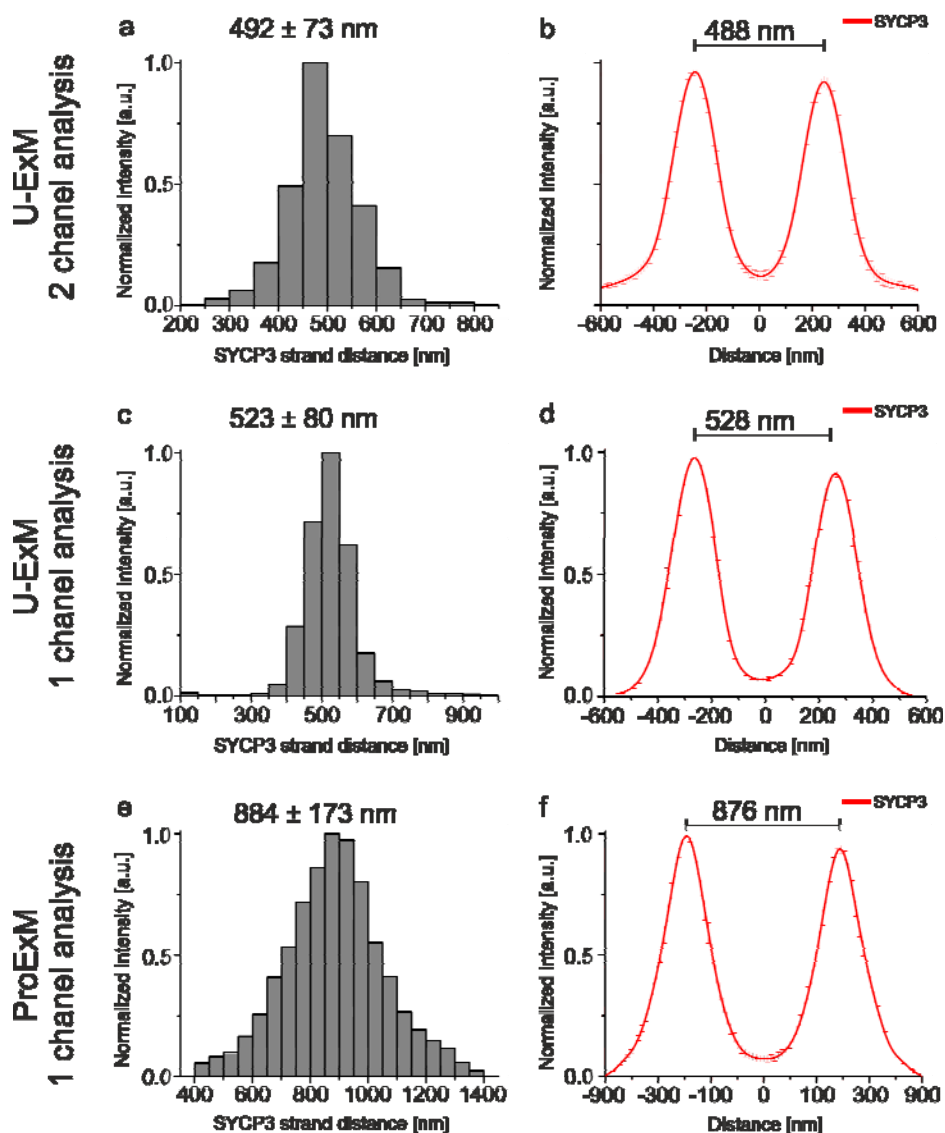
Supplementary Figure 5. a, Histogram of SYCP3 distances determined from U-ExM experiments. The mean distance has been determined to 492 ± 73 nm (SD) from 3,528 intensity line profiles of 24 expanded SCs from two separate expansion experiments. The SYCE3 channel was used to align the line profiles. **b,** Averaged intensity profiles of SYCP3 (red) of U-ExM data from (a). **c-d,** Same data as in (**a**). Here, the SYCP3 channel was used to align the line profiles. The mean distance has been determined to 523 ± 80 nm (SD) from 3528 intensity line profiles of 24 expanded SCs from two separate expansion experiments. **d,** Averaged intensity profiles of SYCP3 (red) of U-ExM data from (c). **e,** Histogram of SYCP3 distances of proExM experiments. The mean distance has been determined to 884 ± 173 nm (SD) from 73427 cross-sectional profiles along 50 expanded SCs. The SYCP3 channel was used to align the line profiles. **f,** Averaged intensity profiles of SYCP3 (red) of proExM data from (e). All data were determined by fitting a bimodal Gaussian function to the histograms. With a bimodal distribution separated by 221nm as measured by *d*STORM (**Fig. 2b,e**) U-ExM enabled post-expansion labeling with various fluorophores and three-color SIM with an expansion factor of ~ 2.4x. On the other hand, proExM provided an expansion factor of ~ 4.0x but pre-expansion labeling resulted generally in a lower labeling density.
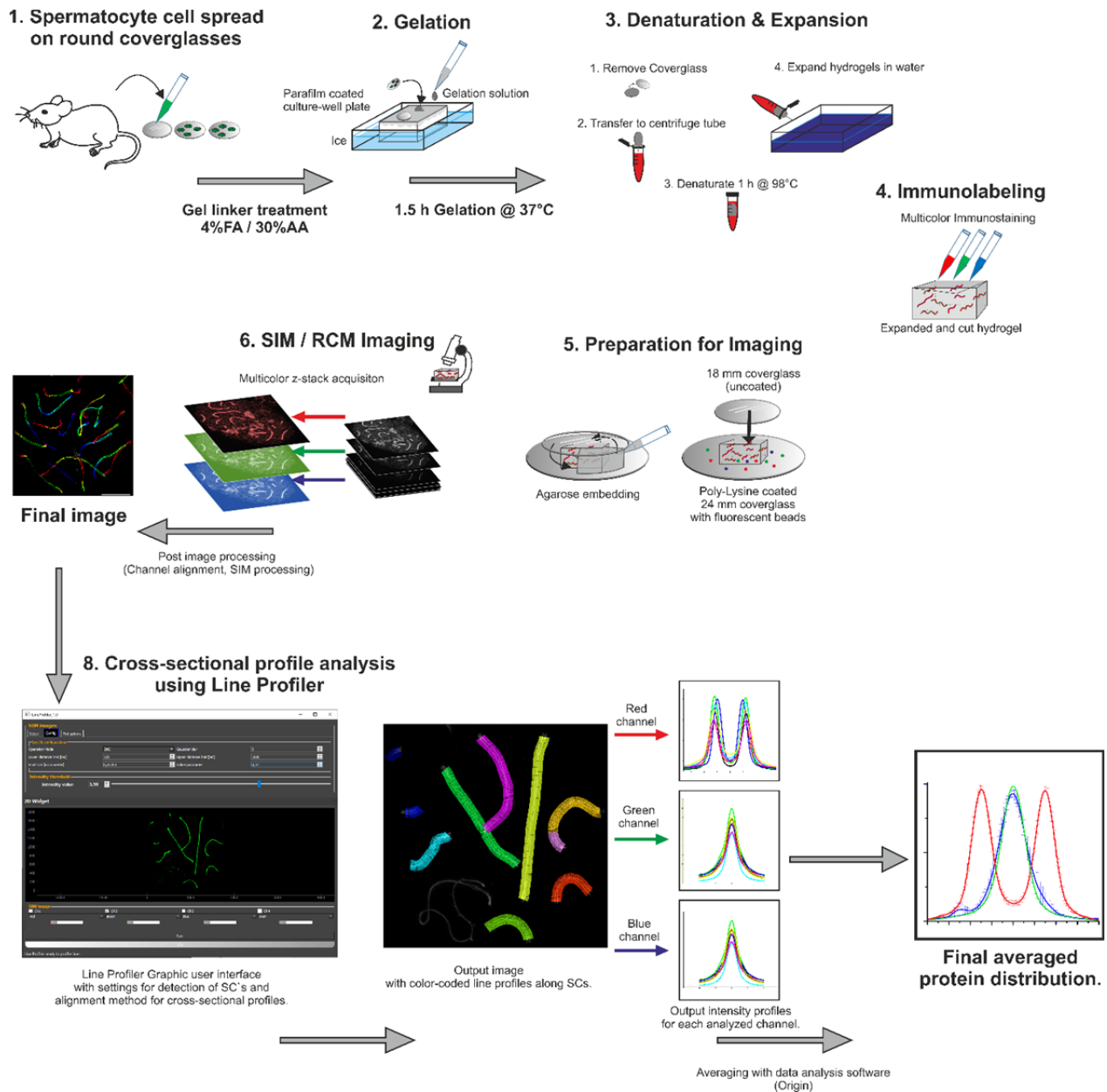
Supplementary Figure 6. Workflow of MAP-SIM expansion on SCs. 1, First, spermatocytes are extracted from mice and then spread on round 18 mm coverslips. **2,** After gel linker treatment, cells are gelated on a parafilm coated culture-well on ice. **3,** Hydrogels are then removed carefully from the coverglass and placed into pre-heated denaturation buffer. After 1 hour of denaturation gels are placed into water for expansion. **4,** Samples are immunolabeled successively with primary and secondary antibodies. **5,** Immunolabeled gels are then immobilized on Poly-Lysine coated coverslips and additionally embedded with agarose to prevent drift during imaging. **6**, Samples can then be imaged with SIM or another available imaging technique. After image acquisition post-processing results in the final images (**7**) of SCs. **8,** Images are then further analyzed using the Line Profiler software enabling analysis of protein distributions in several channels. After averaging of cross-sectional profiles a final averaged protein distribution curve is generated.

973

974 **Supplementary Video 1. 3D-Multicolor MAP-SIM of SYCP3, SYCP1 N-terminus, and**
975 **SYCE3.**
976 Expansion microscopy (MAP) of synaptonemal complex (SC) proteins imaged with structured
977 illumination microscopy (SIM). SYCP3 of the lateral element labeled with Setau647 (red), the N-
978 terminus of transverse filament protein SYCP1 labeled with Alexa 488 (green) and SYCE3 of the
979 central element labeled with Alexa 568 (magenta) on a nuclear spreading shown in pachynema.
980 The xy pair can be distinguished by the short synapsed pseudoautosomal region indicated by
981 the presence of all three SC proteins and the larger unsynapsed parts of the x and the y pair that
982 are only associated with SYCP3. The movie sequence shows the progression through the
983 acquired z-stack. SYCP3, SYCP1N and SYCE3 of the triple immunolocalization are further
984 shown separately to provide better visibility of details of the SC's molecular architecture revealed
985 by MAP-SIM. Note, e.g., that zoomed-in views of the areas where the SC twists (lateral view),
986 suggest a complex architecture of the central element where SYCE3 and the SYCP1 N-terminus
987 reside.

988

989

990 **Supplementary Video 2. Structural details of the SC lateral element revealed by MAP-SIM**
991 **of SYCP3.** Movie sequence showing the expanded lateral element protein SYCP3 (red, labeled
992 with Setau647) of two SCs in pachynema. Note the fraying of the SYCP3 signal at both ends
993 and the occasional bifurcation of the signal along the length of the SC that is in agreement with
994 EM findings of sub-lateral elements (subLEs) in murine spreadings[38].

995

996